JACS
JOURNAL OF THE AMERICAN CHEMICAL SOCIETY

Subscriber access provided by American Chemical Society

Article

Modulation of Calcium Oxalate Monohydrate Crystallization by Citrate through Selective Binding to Atomic Steps

S. Roger Qiu, Andrzej Wierzbicki, E. Alan Salter, Salvador Zepeda, Chris A. Orme, John R. Hoyer, George H. Nancollas, Anita M. Cody, and James J. De Yoreo

J. Am. Chem. Soc., **2005**, 127 (25), 9036-9044• DOI: 10.1021/ja043591s • Publication Date (Web): 03 June 2005

Downloaded from http://pubs.acs.org on March 25, 2009

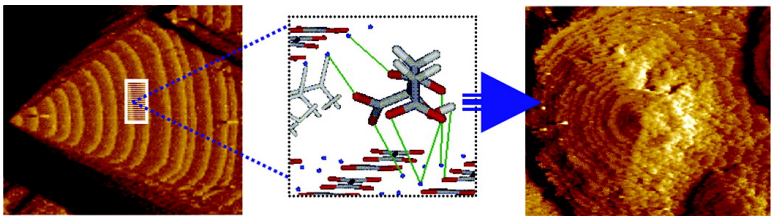

More About This Article

Additional resources and features associated with this article are available within the HTML version:

- Supporting Information
- Links to the 9 articles that cite this article, as of the time of this article download
- Access to high resolution figures
- Links to articles and content related to this article
- Copyright permission to reproduce figures and/or text from this article

View the Full Text HTML

ACS Publications
High quality. High impact.

Journal of the American Chemical Society is published by the American Chemical Society. 1155 Sixteenth Street N.W., Washington, DC 20036

J|A|C|S
ARTICLES
Published on Web 06/03/2005

Modulation of Calcium Oxalate Monohydrate Crystallization by Citrate through Selective Binding to Atomic Steps

S. Roger Qiu,*,† Andrzej Wierzbicki,‡ E. Alan Salter,‡ Salvador Zepeda,†,§ Chris A. Orme,† John R. Hoyer,|| George H. Nancollas,⊥ Anita M. Cody,# and James J. De Yoreo†

Contribution from the Department of Chemistry and Materials Science, Lawrence Livermore National Laboratory, P.O. Box 808, Livermore, California 94551, Department of Chemistry, University of South Alabama, Mobile, Alabama 36688, Department of Chemical Engineering and Materials Science, University of California, Davis, California 95615, The Children's Hospital of Philadelphia, University of Pennsylvania, Philadelphia, Pennsylvania 19104, Chemistry Department, Natural Sciences Complex, University at Buffalo, State University of New York, Amherst, New York 14260, and Department of Geological and Atmospheric Sciences, Iowa State University, Ames, Iowa 50011

Received October 21, 2004; E-mail: qiu2@llnl.gov

Abstract: The majority of human kidney stones are composed primarily of calcium oxalate monohydrate (COM) crystals. Thus, determining the molecular modulation of COM crystallization by urinary constituents is crucial for understanding and controlling renal stone disease. A comprehensive molecular-scale view of COM shape modification by citrate, obtained through a combination of in situ atomic force microscopy and molecular modeling, is presented here. We find that while the most important factors determining binding strength are coordination between COO^- groups on citrate and Ca ions in the lattice, as well as H-bonds formed between the OH group of citrate and an oxalate group, the nonplanar geometry of the steps provides the most favorable environment due to the ability of the step-edge to accommodate all $Ca-COO^-$ coordinations with minimal strain. However, binding to all steps and terraces on the (010) face is much less favorable than on the $(\bar{1}01)$ face due to electrostatic repulsion between oxalate and COO^- groups. For example, the maximum binding energy, -166.5 kJ mol^{-1}, occurs for the [101] step on the $(\bar{1}01)$ face, while the value for the [021] step on the (010) face is only -56.9 kJ mol^{-1}. This high selectivity leads to preferential binding to steps on the $(\bar{1}01)$ face that pins step motion. Yet anisotropy in interaction strength on this face drives anisotropic changes in step kinetics that are responsible for shape modification of macroscopic COM crystals. Thus, the molecular scale growth kinetics and the bulk crystal habit are fully consistent with the simulations.

Introduction

Calcium oxalate monohydrate (COM, $CaC_2O_4 \cdot H_2O$), the most thermodynamically stable form of calcium oxalate (CaOx) crystals, is the primary constituent of the majority of human kidney stones.[1] Although normal urine is often supersaturated with respect to calcium oxalate, human kidney stone formation is usually suppressed by urinary inhibitors[2−4] such as citrate, magnesium, osteopontin, and Tamm-Horsfall protein. Although a few initial molecular-scale investigations of the controlling mechanisms of kidney stone formation by these inhibitory molecules have been recently performed,[5−9] the majority of previous studies have been concerned with the overall kinetics of crystallization, rather than molecular mechanisms which remain poorly defined. An essential requirement for improved understanding is determination of the stereochemical relationships between inhibitors and structural features of the COM surface, the energetic consequences of the interactions with these features, and the impact of these interactions on the kinetics and thermodynamics of COM growth. More generally, the challenge of understanding these relationships and consequences are central to the broader field of biomineralization. Herein, the first comprehensive description of the molecular mechanism by

† Lawrence Livermore National Laboratory.
‡ University of South Alabama.
§ University of California.
|| University of Pennsylvania.
⊥ University at Buffalo, SUNY.
Iowa State University.

(1) Coe, F. L.; Parks, J. H.; Asplin, J. R. *New Eng. J. Med.* **1992**, *327*, 1141−1152.
(2) Hess, B.; Nakagawa, Y.; Coe, F. L. *Am. J. Physiol.* **1989**, *257*, F99−F106.
(3) Asplin, J. R.; Arsenault, D.; Parks, J. H.; Coe, F. L.; Hoyer, J. R. *Kidney Int.* **1998**, *53*, 194−199.
(4) Pak, C. Y. C. *Miner. Electrolyte Metab.* **1994**, *20*, 371−377.
(5) Shirane, Y.; Kurokawa, Y.; Miyashita, S.; Komatsu, H.; Kagawa, S. *Urol. Res.* **1999**, *27*, 426−431.
(6) Guo, S.; Ward, M. D.; Wesson, J. A. *Langmuir* **2002**, *18*, 4284−4291.
(7) Qiu, S. R.; Wierzbicki, A.; Orme, C. A.; Cody, A. M.; Hoyer, J. R.; Nancollas, G. H.; Zepeda, S.; Yoreo, J. J. D. *Proc. Natl. Acad. Sci. U.S.A.* **2004**, *101*, 1811−1815.
(8) Jung, T.; Sheng, X.; Choi, C. K.; Kim, W.; Wesson, J. A.; Ward, M. D. *Langmuir* **2004**, *20*, 8587−8596.
(9) Sheng, X.; Jung, T.; Wesson, J. A.; Ward, M. D. *Proc. Natl. Acad. Sci. USA* **2005**, *102*, 267−272.

10.1021/ja043591s CCC: $30.25 **© 2005 American Chemical Society**

which citrate molecules modify the growth shape of COM is provided. The results allow us to address two important questions about bio-organic control of mineralization: what are the relative roles of the interactions between growth modifiers and newly expressed faces verses step-edge sites on preexisting facets? What structural and chemical aspects of modifier−mineral interaction determine the mechanism and degree of modification?

Citrate was chosen for this study for several reasons. First, because citrate deficiency in the urinary tract is often found in stone formers,[4] a fundamental understanding of how citrate affects the growth of COM can provide insights into the role that citrate plays in kidney stone pathogenesis. Second, a physiochemical understanding of such a role may uncover new avenues for more effective therapy of renal stone disease.[4] Third, because citrate is a small molecule, it is amenable to molecular modeling. Finally, citrate is both nonplanar and contains three carboxylic groups, making it an excellent model for developing insights based on simulations into the role of the acidic peptides and proteins that are considered to be important modulators of biomineralization. From this last perspective, delineation of the molecular modification of COM by citrate may also provide clues into new strategies for biomimetic synthesis of other inorganic crystals.

Previously, we reported the results of a preliminary study utilizing in situ atomic force microscopy (AFM) and molecular modeling to investigate the interaction of citrate with COM crystals.[7] Here, we present a comprehensive description of the experimental results, including the dependence of growth hillock morphology on citrate concentration and the kinetic coefficient for step motion on the $(\bar{1}01)$ face. We further show that the morphological evolution of the growth hillocks mimics the changes in bulk crystal habit in the presence of citrate molecules. We also present the results of extensive molecular modeling that link the AFM observations with the energetics of citrate−COM interactions. We examine the steric match and bonding configuration for a wide range of steps and terraces to understand the stereochemical source of citrate modification of COM. Our molecular modeling results are completely consistent with experimental observations. These results have two significant impacts. First, they demonstrate that, even for a complex organic modifier with multiple functional groups, step-specific interactions at the molecular level on preexisting atomic steps directly control the modification of bulk crystal habit. Second, they provide the first detailed pictures of the stereochemistry that leads to such control including the role of electrostatic interactions, hydrogen bonding, and steric match.

Method and Experimental Procedures

The COM crystals used for these studies were grown in vitro by a gel method similar to that described in ref 10. For in situ AFM experiments in aqueous solution, supersaturated $CaC_2O_4 \cdot H_2O$ solutions (calcium-to-oxalate ratio = 1) were prepared using reagent grade $K_2C_2O_4$ and $CaCl_2 \cdot 2H_2O$. Relative supersaturation, defined as $S = (a(Ca^{2+}) \cdot a(C_2O_4^{2-})/K_{sp})^{\wedge} 0.5 - 1$, where $a(Ca^{2+})$ and $a(C_2O_4^{2-})$ are the activities of the calcium ion and oxalate ion, respectively, and K_{sp} ($=1.66 \times 10^{-9}$ M^2)[11] is the solubility product for COM at room temperature, was varied from 0.1 to 1.1, which are within the physiological range.[12,13] The pH of all solutions was adjusted to 7.0 before each experiment. Stock citrate solution was added to the supersaturated salt solutions for the additive-bearing experiments. Citrate concentrations ranged from 0.01 to 0.1 mM, which is somewhat lower than the physiological range.[13,14] All in situ images were collected at room temperature (24 °C) in contact mode (DI, Nanoscope III, Santa Barbara, CA) on surfaces of the COM crystals that were anchored inside the enclosed fluid cell. The images were obtained while supersaturated solutions were flowing through the system. The flow rate (2 mL/min) was adjusted to ensure that growth was limited by surface kinetics and not by diffusion. Using this criteria, at a given supersaturation, the step speed did not change when the flow rate was further increased.[15]

To ensure that the AFM images were authentic representations of the surface morphology, several precautions were taken. First, the imaging force was reduced to the minimum possible value that allowed the tip to remain in contact with the surface so that there was no measurable effect of imaging on the growth kinetics. We verified this by gradually increasing the force until effects on the morphology and step speed were observed or by zooming out to a larger scan box and looking for the signature of the smaller scan area. A consequence of imaging in this regime is that sometimes the tip can transiently pull off the surface. This reduces image quality but ensures that the morphology and kinetics of the steps are minimally affected. Next, images were also collected at different scan angles and trace and retrace images were regularly compared, to eliminate the possibility of imaging artifacts induced by tip contamination or tip sticking. Furthermore, step speed was estimated from both images collected at a larger and smaller scale to ensure there was no effect of scanning. Because the in situ images were taken in real time, it is inevitable that distortion of the step-orientation will exist in the images. Such distortion is caused by the step movement during the finite scan time so that its apparent direction differs from the true orientation. The images reported here were not corrected for this effect. In fact, we use this change in angle to extract the step velocities at different growth conditions.[16]

To model the strength of molecular interactions, energy minimizations were applied to the citrate/COM system using the Universal Force Field (UFF) 1.02.[17] The water solvation effect was incorporated by setting the dielectric constant to 80. The optimization procedure takes into account the contributions from electrostatic forces, van der Waals forces, hydrogen bonds, bonds, bond angles, and dihedral angles to the total energy of the system. During the calculation, we first optimized the initial structure of citrate molecule using the ab initio Hartree−Fock method[18] (6-31+G(d,p) basis set). The atomic charges used for citrate in this study were obtained by fitting to molecular electrostatic potentials[19−21] using Spartan software for electronic calculations (Spartan 5.1.1, Wave function Inc., Irvine, CA). The coordinates of lattice atoms were kept fixed, and the citrate molecule was allowed to translate, rotate, and adopt any conformation on the surface of COM. For each configuration, we exhausted all possible initial citrate docking positions. Each time we had one of two outcomes. Either the molecule returned to the minimum already determined, or, on occasion, it became fixed in a different orientation for which the binding energy was significantly smaller. The latter cases represent local energy minima; however, only the global minima are reported in this paper. The binding energies of citrate were determined by taking the difference between the optimized energy of the system in which citrate is bound to the

(10) Cody, A. M.; Horner, H. T.; Cody, R. D. *Scanning Electron Microsc.* **1982**, *Pt1*, 185−197.
(11) Tomazic, B. B.; Nancollas, G. H. *Invest. Urol.* **1979**, *16*, 329−335.
(12) Robertson, W. G. *Clin. Chim. Acta* **1969**, *24*, 149.
(13) Robertson, W. G.; Peacock, M.; Nordin, B. E. C. *Clin. Sci.* **1968**, *34*, 1968.
(14) Elliot, J. S. *Invest. Urol.* **1964**, *1*, 582.
(15) Gilmer, G. H.; Ghez, R.; Cabrera, N. *J. Cryst. Growth* **1971**, *8*, 79−93.
(16) Land, T. A.; De Yoreo, J. J.; Lee, J. D. *Surf. Sci.* **1997**, *384*, 136−155.
(17) Rappe, A. K.; Casewit, C. J.; Colwell, K. S.; Goddard, W. A., III; Skiff, W. M. *J. Am. Chem. Soc.* **1992**, *114*, 10024−10035.
(18) Hammer, B.; Hansen, L. B.; Norskov, J. K. *Phys. Rev. B* **1999**, *59*, 7413−7421.
(19) Breneman, C. M.; Wiberg, K. B. *J. Comput. Chem.* **1990**, *11*, 361−373.
(20) Chirlian, L. E.; Francl, M. M. *J. Comput. Chem.* **1987**, *8*, 894−905.
(21) Payne, M. C.; Teter, M. P.; Allan, D. C.; Arias, T. A.; Joannopoulos, J. D. *Rev. Mod. Phys.* **1992**, *64*, 1045−1097.

COM surface and the sum of citrate and COM energies when separated beyond the interaction distance. Optimization calculations were run until convergence criteria, typical for this class of crystals, were met. Note that vacuum ab initio simulations were also carried out as part of this study; while giving values that are far too large because they do not include the effect of the dielectric constant of water, they produced values that increase in the same order as for the UFF calculations.

Models of the flat and stepped surfaces of COM were built using Cerius[2] (Accelrys Inc., San Diego, CA) Surface Builder (Version 4.2MS) from the unit cell derived from the crystallographic data.[22] Because hydrogen atoms were not included in the unit cell in ref 22, their positions were determined computationally by CASTEP (Accelrys Inc., San Diego, CA) at the GGA-RPBE[4] level of theory. Three-dimensional periodic boundary conditions were applied to the COM unit cell. The dimensions of the cell were fixed at its crystallographically determined values, and all atoms within the unit cell were frozen except the hydrogen atoms, which were free to move. The electrostatic charges on the COM system were also assigned by fitting to molecular electrostatic potentials.[19−21]

COM Crystal Structure

COM is a monoclinic crystal with a $P2_1/n$ space group and unit cell parameters of a 9.976 Å, b 14.588 Å, c 6.291 Å, and β 107.05°.[22] The shape and size of these crystals depend on the growth conditions such as ionic strength, pH, temperature, and local environment.[10,23−27] While most of the synthetic COM crystals exhibited habits with three distinct faces, the {$\bar{1}$01}, {010}, and {120}, with aspect ratios similar to those shown in Figure 1a, crystal habits with different aspect ratios were also reported under other growth conditions, where {021} faces have also been observed.[8,9,23] The habits of the seed crystals used in our studies are similar to those displayed in Figure 1a, with the ($\bar{1}$01) and (010) faces being the object of this investigation.

The molecular structures of the two faces are also shown in Figure 1c,d. For ease of viewing, the molecular coordinates are slightly shifted with respect to their correct positions on both faces, and on the ($\bar{1}$01) face, oxalate groups at the edge are only partially displayed. In both planes, the surface layers contain two sublayers of oxalate groups; one is parallel and the other is perpendicular to the planes, respectively. While the perpendicular oxalate groups on the ($\bar{1}$01) plane lie below the topmost surface layer, those on the (010) plane are exposed and extend beyond the plane. The structural differences make the ($\bar{1}$01) plane richer in Ca^{2+} than the (010) plane and, as discussed later, dictate the strength of their interactions with solution additives to which both faces are exposed during crystal growth.

On the ($\bar{1}$01) plane, the molecular rows stack in repeating sequences of AA′BB′AA′ (Figure 1c). As we will show below, this stacking sequence leads to step bunching and step interlacing on the (010) surface. If the water molecules in the COM structural models are replaced by oxygen atoms, a common simplification, significant steric features associated with the water molecules vanish. This omission gives rise to an AAB-BAA stacking sequence of molecular rows on the ($\bar{1}$01) plane. Because the molecular stacking sequence has implications for both step dynamics and hillock structure, this clear difference between the models with and without oxygen atoms shows the importance of including the entire water molecule in structural models to correctly interpret AFM data. These implications are considered in greater detail in the following discussion.

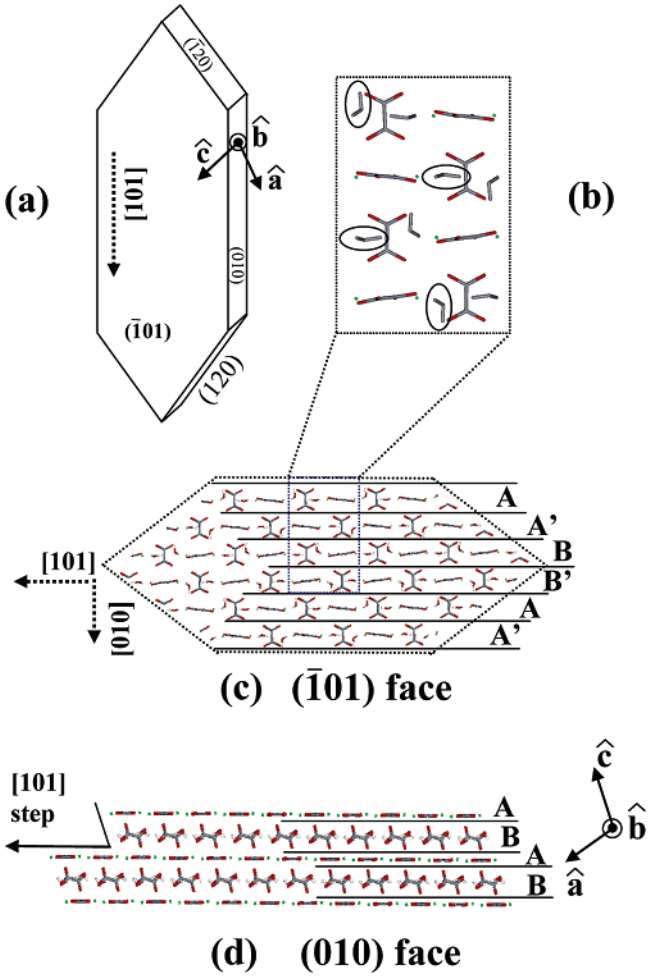

Figure 1. (a) Schematic of COM crystal habits showing the three commonly expressed planes ($\bar{1}$01), (010), and {120}. The coordinate unit vectors a, b, and c for the monoclinic system are also displayed. The symbol ⊙ indicates that the b axis points out of the (010) face. (b) Enlarged views of the molecular structure of the ($\bar{1}$01) surface showing the different orientations of water molecules in successive rows as indicated in (c). For ease of viewing, the water molecules are shaded in gray. The circled water molecules highlight the steric differences in each of the four rows. (c) Molecular structure and stacking layers of the COM ($\bar{1}$01) surface viewed along the [00$\bar{1}$] direction. The dotted hexagon shows the relationship between crystal habit and molecular structure. Solid lines emphasize the AA′BB′ stacking sequence that is perpendicular to the [010] direction. (d) Molecular structure of the (010) face. Also shown is the [101] step on the ($\bar{1}$01) face viewed down the [010] axis. Solid lines show the AB stacking in the (010) plane. Green, Ca^{2+}; red, O; dark grey, C; off-white, H.

The stacking sequence on the (010) plane is much simpler than on the ($\bar{1}$01) plane. As shown in Figure 1d, there are only two distinct molecular layers in the repeating structural unit, A and B. This two-layer molecular structural unit suggests that for the elementary step along the [101] direction on the ($\bar{1}$01) face, there are three possible step heights, 2.4, 4.9, and 6.3 Å, with the latter containing both sublayers.

Results and Discussion

(1) AFM Measurements. (a) Pure Solution. COM crystals grew on complex screw dislocation hillocks comparable to those

(22) Deganello, S.; Piro, O. *Neues Jahrb. Mineral., Monatsh.* **1981**, *2*, 81−88.
(23) Millan, A. *Cryst. Growth Des.* **2001**, *1*, 245−254.
(24) Webb, M. A. *Plant Cell* **1999**, *11*, 751−761.
(25) Gvozdev, N. V.; Petrova, E. V.; Chernevich, T. G.; Shustin, O. A.; Rashkovich, L. N. *J. Cryst. Growth* **2004**, *261*, 539.
(26) Wierzbicki, A.; Sikes, C. S.; Sallis, J. D.; Madura, J. D.; Stevens, E. D.; Martin, K. L. *Calcif. Tissue Int.* **1995**, *56*, 297−304.
(27) Shirane, Y.; Kagawa, S. *J. Urol.* **1993**, *150*, 1980−1983.

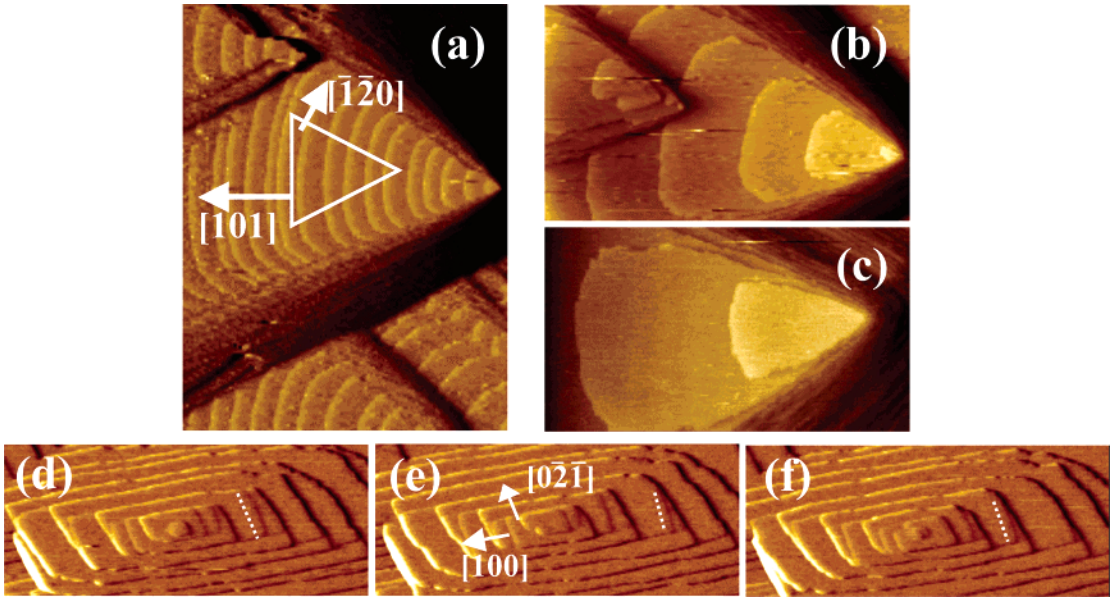

Figure 2. AFM images showing the morphology of the COM growth hillocks. (a−c) Growth hillocks on the ($\bar{1}01$) face at different scales. (d−f) Growth hillocks on the ($0\bar{1}0$) face (equivalent to (010) face by symmetry). The white dotted lines in sequential images (t = 0 (d), t = 200 s (e), and t = 380 s (f)) show the process of step interlacing during growth. Horizontal dimension: (a) 10 μm; (b) 5.5 μm; (c) 2.4 μm; (d−f) 1.6 μm.

of many other solution grown crystals such as KDP[28] and calcite.[29] Within the ranges of supersaturation used (S = 0.1−1.1), 2-D nucleation was not observed. The growth hillock density was much higher on the ($\bar{1}01$) face than on the (010) face. In general, crystals grew mainly on a few dominant hillocks with other minor sources emerging on the flanks of these hillocks. Representative examples of growth hillocks on both the ($\bar{1}01$) and the (010) faces are shown in Figure 2a−c and Figure 2d−f, respectively.

($\bar{1}01$) Face. Growth hillocks on the ($\bar{1}01$) face exhibited a triangular-shaped morphology that is quite different from its equilibrium hexagonal habit. Steps propagating toward the {010} faces and the ($1\bar{2}0$) and (120) were not present. Instead, steps moving toward [101] were observed that truncate the angle formed by the [$\bar{1}\bar{2}$0] and [$\bar{1}$20] directed steps. The implication is that steps directed toward these three unrepresented directions have considerably higher speeds than the others. Even so, for growth at S = 0.8, [101] directed steps move at about 10 nm/s, which is already 12 times faster than that of the other two. This means that there is a huge anisotropy in step speed or attachment/detachment kinetics between the [$1\bar{2}$0]/[120] and [$\bar{1}\bar{2}$0]/[$\bar{1}$20] directions, despite the fact that the only significant difference is in the tilt angle of the oxalates (Figure 1c). The highly anisotropic step kinetics gives rise to closely spaced steps along the two slower directions as shown in Figure 2a−c. Although double steps are observed at some hillocks, the majority of the hillocks have only single steps with a height of 6 Å, implying that either the growth unit contains two molecular sublayers as described earlier or the addition of one type of unit occurs on a time scale which is short as compared to the time required for growth units of the other type.

Based on the measured step speed for growth at S = 0.82 and the assumption of linear dependence of step speed on solute concentration[30,31] (this linear dependence has been observed for many systems and is rationalized by considering the balance between attachment/detachment at steps under an applied flux[30]), we calculate the kinetic coefficient, $\mathscr{K}_{101}$, $\mathscr{K}_{-1-20}$, and $\mathscr{K}_{100}$ to be 0.2, 0.02, 0.03 cm s^{-1}, respectively, with $\mathscr{K}$ defined by $v = \omega\mathscr{K}(C - C_e)$, where v is the step speed, ω is the molecular volume of the solid (=1.1 × 10^{-22} cm^3 molecule), and $C - C_e$ is the difference between the actual and equilibrium Ca^{2+} concentrations, the latter calculated from the K_{sp} for COM. These values are similar to those found for other inorganic salts.[30,31]

(010) Face. The geometry of growth hillocks on the (010) face exhibited a near rectangular-shaped morphology bound by ⟨100⟩ and ⟨021⟩ steps.[32] Over the range of supersaturations, the step speed along ⟨100⟩, 1.2 nm/s at S = 0.82, was about 1.5 times faster than that along ⟨021⟩. The absence of ⟨$\bar{1}$01⟩ steps suggests that these steps have considerably higher step speeds and are therefore unexpressed. Moreover, AFM images show that the growth sources are rather complicated and contain multiple screw dislocations, often of the Frank−Reed type.[33]

For the first couple turns of the growth spiral, the step heights range from 1 to 3 h, where h is the height of an elementary step, about 3.98 Å. However, at a sufficient distance away from the dislocation source, all steps are quadrupled with heights of ca. 16 Å. This quadrupling of steps is caused by, so-called, "step interlacing",[34,35] which is most apparent at the hillock corners as shown in Figure 2d−f. Both the step interlacing and the step bunching have their origin in the AA′BB′ packing sequence described above. This packing structure creates a screw-axis symmetry element perpendicular to the (010) face and leads to

(28) Rashkovich, L. N. *KDP-family Single Crystal*; Adam Hilger: New York, 1991.
(29) Teng, H. H.; Dove, P. M.; Yoreo, J. J. D. *Geochim. Cosmochim. Acta* **2000**, *64*, 2255−2266.
(30) De Yoreo, J. J.; Vekilov, P. G. In *Biomineralization*; Dove, P. M., Yoreo, J. J. D., Weiner, S., Eds.; Mineralogical Society of America Geochemical Society: Washington, DC, 2003; Vol. 54, pp 57−93.
(31) Chernov, A. A. *Sov. Phys. Uspekhi* **1961**, *4*, 116−148.
(32) [*UVW*] specify a unique vector direction, and ⟨*UVW*⟩ represent a set of vector equivalent by symmetry.
(33) Frank, F. C.; van der Merwe, J. H. *Proc. R. Soc. London* **1949**, *A198*, 205.
(34) Frank, F. C. *Philos. Mag.* **1951**, *42*, 1014.
(35) van Enckevort, W. J. P.; Bennema, P.; van der Linden, W. H. *Z. Phys. Chem. Neue Folge* **1981**, *124*, 171.

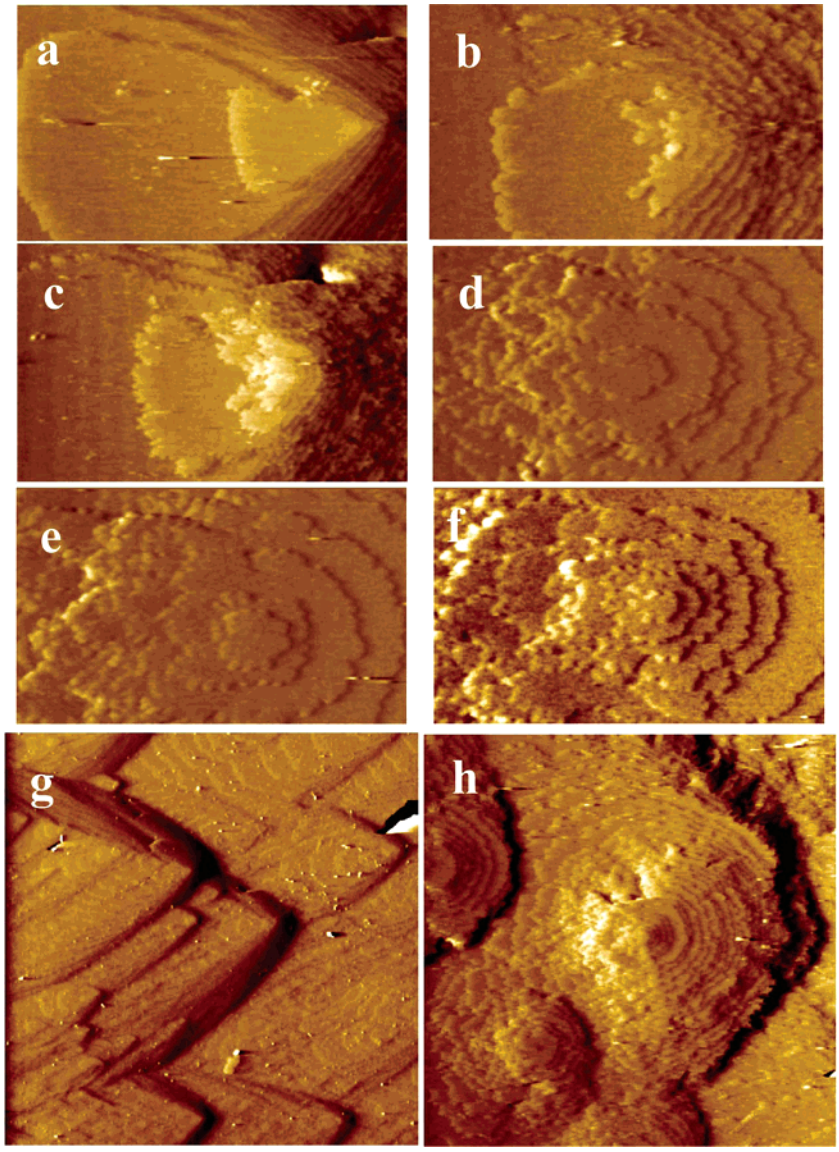

Figure 3. Morphological changes of COM growth hillocks due to the presence of citrate. (a−f) Sequential AFM images showing the evolution of the dislocation hillocks during growth in citrate-bearing solution (molar citrate-to-calcium ratio: 0.1) at $t = 0$ min (a), $t = 5$ min (b), $t = 10$ min (c), $t = 65$ min (d), $t = 80$ min (e), $t = 100$ min (f). (g−h) Larger scale AFM images show the drastic alteration of growth morphology due to the citrate. (g) Multiple growth hillocks on the $(\bar{1}01)$ surface in pure solution displaying the representative triangular morphology. (h) Final shape of hillocks after the citrate effect is fully realized. Horizontal dimension: (a, c) 1.5 μm; (b, d−f) 1.0 μm; (g) 20 μm; (h) 4 μm.

asymmetries in step speed from layer to layer with a 4-layer periodicity.

In Figure 1b, the AA′BB′AA′ stacking sequence of the molecular rows in the $(\bar{1}01)$ plane comprise the elementary steps that define sequential terraces of hillocks on the (010) face. There are two types of water molecules and oxalate groups within these rows: type 1 lying flat and type 2 perpendicular to the $(\bar{1}01)$ plane. The orientation of the type 2 oxalate groups, and calcium pairs in layers A and A′ are the same and are mirrored by their counterparts in layer B and B′. The water molecules, on the other hand, are different in all four molecular layers, although they are related by a symmetry operation. On the (010) face, this structural switch results in small differences in step speeds among the layers. Because the faster steps eventually catch up to slower steps as indicated by the white lines in Figure 2d−f, after only a few turns of the dislocation spiral, step bunches displaying the periodicity of the AA′BB′ stacking are generated. Thus, the unique stacking structure along with the change in orientation about the screw-axis at the A/B′ interface leads to growth of the (010) face on quadruple height steps.

(b) Citrate-Doped Solution. $(\bar{1}01)$ Face. Both step morphology and kinetics were significantly altered on the $(\bar{1}01)$ face when citrate was present in solution (Figure 3). Moreover, both the magnitude of the effect and the rate at which the full effect was observed increased with citrate concentrations. Step speeds were reduced and step edges became roughened. Both the changes in speed and roughness depended on step direction.

The temporal evolution of the $(\bar{1}01)$ face after introduction of citrate (citrate: 1.2×10^{-5} M, $S = 0.7$) is shown in Figure 3a−d. Shortly after citrate was introduced, the step speed along all directions was gradually decreased. By the time the full effect was realized, the speed along [101] was reduced by a factor of 25, while the speeds along $[\bar{1}20]$ and $[\bar{1}\bar{2}0]$ were only reduced by a factor of 2.

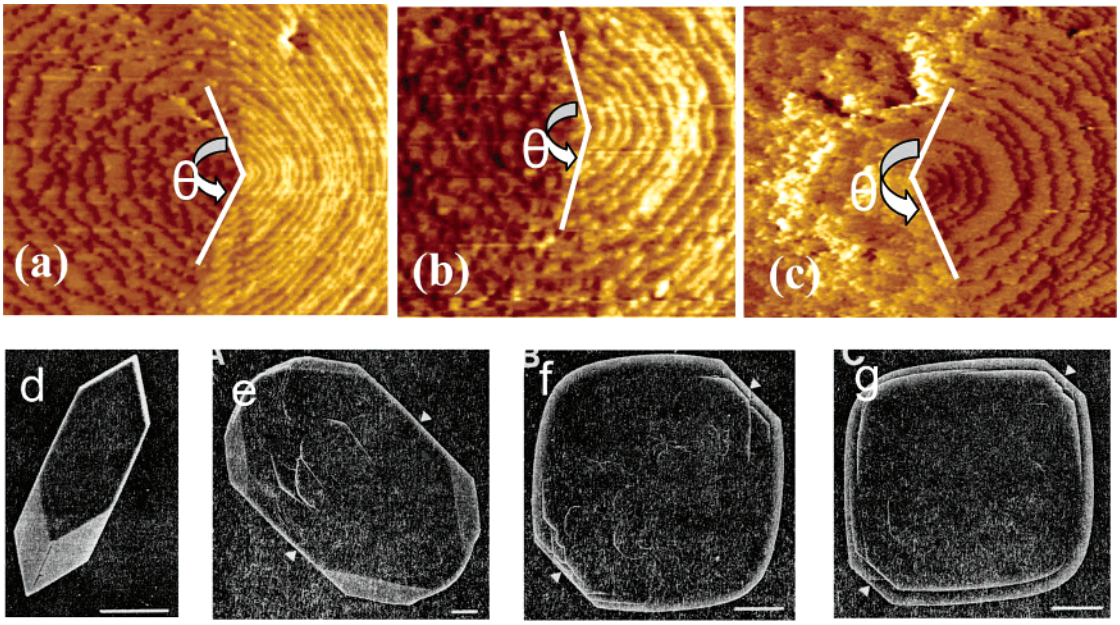

Figure 4. (a−c) AFM images showing the final morphology of the growth hillocks at three different citrate levels. Total calcium concentration for all three solutions is 1.2×10^{-4} M. Molar citrate-to-calcium ratios ratio are 0.02 (a), 0.04 (b), and 0.1 (c). Image horizontal dimension: (a) 4 μm, (b) 2 μm, (c) 1 μm. (d−g) Scanning electron micrographs of COM crystals formed in pure supersaturated calcium oxalate solution (d) and in the citrate-bearing solutions at various citrate concentrations: 10^{-4} M (e), 10^{-3} M (f), and 2×10^{-3} M (g). Scale bar: 10 μm (reprinted with permission from *Journal of Urology*, ref 27).

Accompanying the drop in step speed was a change in step and growth hillock morphology. Step edges along all three directions were roughened due to the presence of citrate, with the most dramatic changes occurring at the [101] step. After a prolonged time, the [101] step lost its stability and presented a highly ramified step front, while $[\bar{1}20]$ and $[\bar{1}\bar{2}0]$ steps evolved to a single half-circle-shaped step with its center coinciding with the dislocation origin. The serrated morphology of the newly expressed step edges suggests that citrate molecules modify COM growth by pinning step motion.[7] The net result of these changes in step speed and shape was to alter the morphology of the growth hillocks from a triangular to a nearly circular shape as shown in Figure 3g,h.

The shape change at the elementary step level due to the addition of citrate is reflected in the macroscopic growth habit that has been reported previously.[26,27] Comparison between our results and bulk crystal growth experiments demonstrates that the evolution of crystal habit with increasing citrate concentration mimics the growth hillock geometry on the $(\bar{1}01)$ face (Figure 4). The final shape of both was directly related to the citrate concentration.

Figure 4a−c shows the final morphology of the growth hillocks at three citrate levels with increasing concentrations. The degree of shape modification can be characterized by the angle θ, defined by the rough/smooth step boundary. The magnitude of θ increases with citrate concentration and is directly determined by the relative step speed along the [101] and $\langle 120 \rangle$ directions. At the macroscopic level, the extent of the change in the crystal habit similarly increases with citrate concentration (Figure 4e−g).[27] Figure 4d shows the crystal habit of COM grown from pure supersaturated calcium oxalate solution.[27] From Figure 4d−g, it is apparent that in citrate-containing solutions, the crystal shape evolves from the hexagonal-like habit to one characterized by the reduction of aspect ratio (length/width), rounding of the $(\bar{1}01)$ face, and reduction of the crystal thickness. Moreover, the decrease in the (010) plane surface area shows that the (010) face is becoming the fastest growing, suggesting that its growth is the least inhibited by the citrate. These observations of the bulk crystal habit are consistent with our AFM measurements. Yet the growth shape of the steps is defined by the orientational dependence of the kinetic coefficient, $\mathscr{K}$, and the side faces themselves become rounded (like the steps) so that true crystallographic planes are no longer expressed. Thus, the close correspondence of the results from both the macro- and the microscales shows that overall crystal shape is being controlled by the elementary step kinetics and not by considerations of minimum surface energy. This conclusion does not, however, rule out the possibility that the step edge and interfacial energies are modified in a similar fashion.

(010) Face. The effect of citrate on the (010) face is minimal. The growth hillocks showed a minor change after citrate was introduced, although a small degree of rounding at two corners of the hillocks was observed. Furthermore, there were no appreciable changes in step speed. Figure 5a−d shows the growth hillocks before and after citrate was added to the solution at different length scale.

(2) Molecular Modeling. To understand the stereospecifity of citrate binding to COM crystals, we employed molecular modeling with energy minimization to calculate binding energies of citrate at steps and surfaces of COM crystals for several possible configurations (listed in Table 1). Previously, Wierzbicki et al.[26] used such models to predict that the binding energy of citrate to the $(\bar{1}01)$ face should be larger than that to the (010) face. However, our calculations show that binding energies to all affected steps are higher than that to either the $(\bar{1}01)$ or the (010) face. Moreover, we find that citrate binds to the [101] step, that is, the one that is most strongly affected, with what is by far the highest binding energy. The binding energies for all possible configurations are summarized in Table 1.

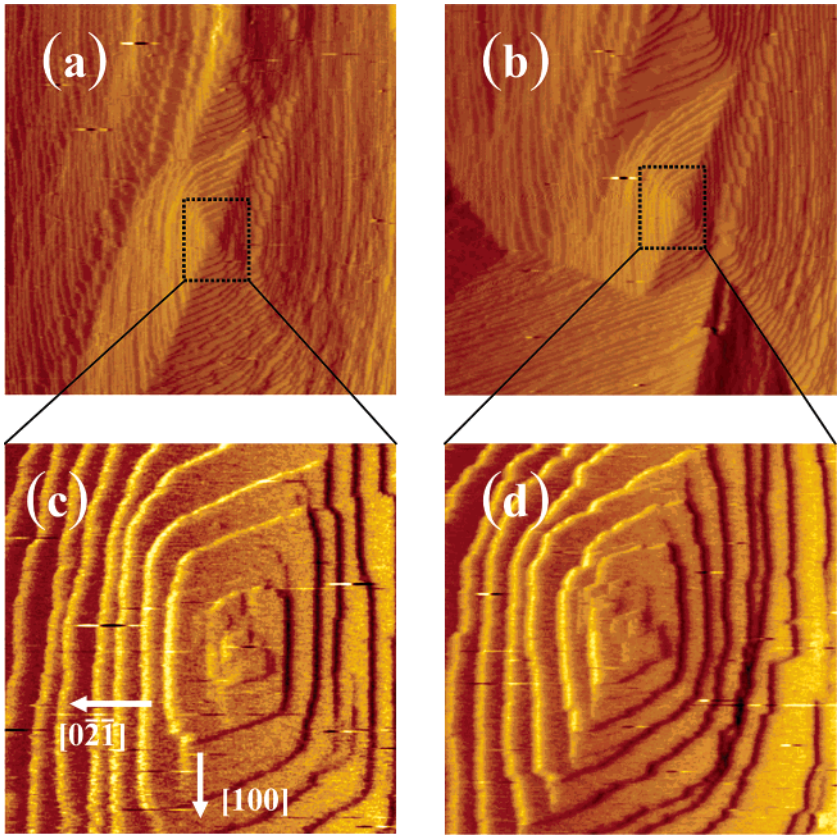

Figure 5. AFM images show the growth hillocks on the (0$\bar{1}$0) face (equivalent to (010) face by symmetry) in pure (a, c) and citrate-containing solutions (b, d). Image sizes are (a) 6 μm, (b) 5 μm, (c−d) 1.2 μm.

Table 1. Binding Energies (kJ mol^{-1}) of Citrate Bound to Various Steps and Faces of COM Crystal

	($\bar{1}$01) face	(010) face
($\bar{1}$01) plane	−65.4	
[101] acute step	−166.5	
[1$\bar{0}$1] obtuse step	−110.0	
[1$\bar{2}$0] obtuse step	−133.8	
[120] acute step	−162.4	
(010) plane		−48.9
[100] straight step		−73.2
[100] obtuse step		−92.8
[021] obtuse step		−56.9
[021] straight step		−102.4

($\bar{1}$01) Face. There are two ways to build the [101] step based on the crystal structure, both of which have the same step base in the ($\bar{1}$01) plane but a different step riser. One is the (100) plane which gives rise to an acute step, while the other is the (101) plane creating an obtuse step. From crystal habit alone, we would predict that the step riser is a microfacet of (100), which is an acute step. Yet, a priori, we have no basis for assuming that at single step level, this configuration is the most stable configuration. The citrate molecule was thus docked to both step structures for energy minimization. The calculation showed binding energies of −166.5 kJ/mol at the acute step but only −110.0 kJ mol^{-1} when bound to the obtuse step. The fact that citrate interacts most strongly with the [101] step as shown by AFM, coupled with the large difference between the binding energies for the possible step configurations, argues that the [101] step is an acute step formed by intersection of the ($\bar{1}$01) and (100) planes, although this evidence is not conclusive.

The specificity of the citrate interaction with the acute [101] step is achieved due to the excellent matching between the separation of carboxylic groups of citrate and the calcium ion distribution in the step (Figure 6). Moreover, the acute geometry allows multiple accommodations of carboxylate groups with the least amount of distortion as the distance between two adjacent calcium ions along the [010] direction is 7.3 Å, which is close to the 7.0 Å distance between the two end carboxylic groups of citrate. Furthermore, the OH group and the middle carboxylic group within the citrate molecule are oriented in a plane that is perpendicular to the axis formed by the backbone carbon chains. Such a configuration makes it possible for them to form bonds with atoms both in the basal and in the riser planes. Figure 6a,b demonstrates from two different view directions the steric recognition by citrate of the acute [101] step as it forms the strongest bonds with this step. The green lines display the bonding between carboxylic and Ca^{2+} ions and the hydrogen bonding between the carboxylic ions and the hydroxyl group on the citrate molecule. This shows that carboxylic groups facilitate the binding of Ca^{2+} ions in both step riser and basal planes when interacting with the crystal face. As seen in the figure, one of the end-carboxylic groups faces down to the basal plane and forms bonds with two Ca^{2+} ions, both of which are in the basal plane. Meanwhile, the other two carboxylic groups interact with Ca^{2+} ions from both of the planes that form the step, and the hydrogen atom from the hydroxyl group forms a hydrogen bond with one of the oxygen atoms within the oxalate ions in the basal plane. In this configuration, the citrate molecule is slightly skewed from [010], which can be caused by the constraints imposed by the distribution of Ca^{2+} ions in the crystal lattice, the rigid bonding between these ions, and the hydrogen bond formation in the basal plane. Because the hydroxyl group

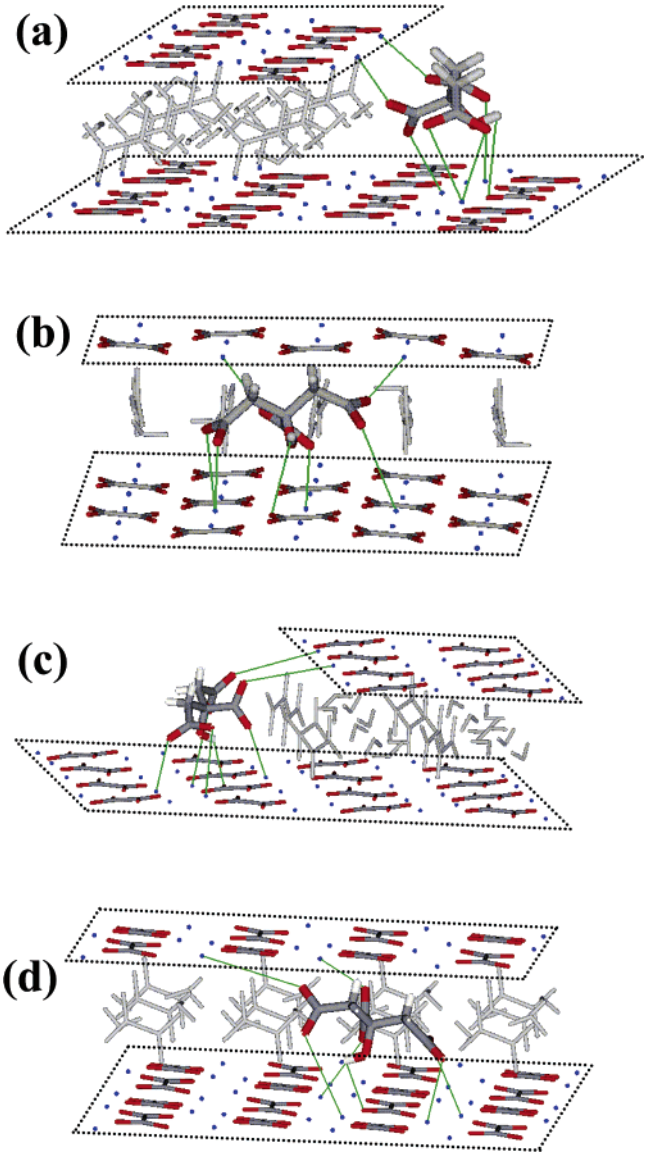

Figure 6. Geometry of citrate binding to steps on the ($\bar{1}$01) face in the minimum energy configuration. For ease of viewing, molecules in the step riser plane are shaded in gray. Chemical bonds between the citrate molecules and calcium ions and between the hydroxyl groups and the oxalate ions are displayed by green lines. (a and b) Citrate bound to the acute [101] step viewed approximately (a) parallel to and (b) perpendicular to the step. Citrate bound to the [$\bar{1}\bar{2}$0] step viewed approximately (c) parallel to and (d) perpendicular to the step. Blue, Ca^{2+}; red, O; dark gray, C; off-white, H.

is rather flexible, it behaves as a pivot to hold the citrate molecule in place and thus stabilize the attachment when it is docked to the acute step.

Our calculations also predict strong bonding between a citrate molecule and the [$\bar{1}\bar{2}$0] step on the ($\bar{1}$01) plane, although the interaction is not as strong as that with the acute [101] step. Based on the molecular packing, the [$\bar{1}\bar{2}$0] step can only be an obtuse step. As shown in Figure 6c, the oxalate group in the step riser extends out of the ($\bar{1}\bar{2}$0) plane. Thus, it is possible for the hydroxyl group to face the ($\bar{1}\bar{2}$0) plane and to form a H-bond with the oxygen atoms in the oxalate group, while the carboxylic groups interact with the Ca^{2+} ions within the step. Alternatively, the hydroxyl could form a H-bond with the oxalate group in the basal plane as described for the [101] step, as these two steps have the same basal planes. However, molecular modeling shows that Figure 6c,d is the strongest possible binding configuration for the interaction between citrate and the obtuse ($\bar{1}\bar{2}$0) step, giving a binding energy of −133.8 kJ/mol. Yet this is still considerably less than for the [101] step, and thus the addition of citrate does not inhibit growth of the [$\bar{1}\bar{2}$0] step to the same degree as the [101] step.

We also calculated the energy of citrate binding to the [120] step, although such a step is not expressed when the crystal is growing under pure supersaturated calcium oxalate solution. This step can only be acute, based on the crystal lattice. The binding energy is ca. −162.4 kJ/mol, which is comparable to that of the acute [101] step. This helps to explain why the step along the [101] direction becomes rounded, first expressing the [120] corners, and then losing stability for all directions between [120] and [1$\bar{2}$0]. Our calculations also show that the strong binding to this step only occurs when hydrogen bonding is possible with the oxalate group in the basal plane.

(010) Face. Binding energies of citrate to steps on the (010) plane are much smaller than those on the ($\bar{1}$01) face, indicating that it is less favorable for citrate to bind to these steps. This is consistent with our AFM observation that citrate has a much lower effect on the modulation of the growth on the (010) face. In general, for all steps on the (010) plane, the smaller binding energy can be attributed to the oxalate groups that extend beyond the (010) plane, which forms the base of all of the steps. Oxygen atoms in these oxalate groups are negatively charged and thus electrostatically repel carboxylic groups in the citrate molecule when citrate binds to the steps. Moreover, the basal plane intersects with the step riser forming a straight step, resulting in poor geometric matching between the Ca^{2+} ions and the nonplanar carboxylic groups. Such a sterically hindered condition can only be satisfied by the distortion of the citrate molecule and a concomitant strain.

The [100] step can either be square if the riser plane is the (100) plane or obtuse if the riser is the (120) surface. For the square step, there are two possible configurations based on the local orientation of the oxalate groups on both the step riser and the basal plane at the intersection of the planes, both of which are either parallel or perpendicular to the (010) plane. The binding energy (−73.2 kJ mol^{-1}) is higher for the step with the oxalate group parallel to the (010) plane, due to the higher Ca^{2+} concentration at the binding location. Note that this binding energy is smaller than the previously reported value.[7] The discrepancy is attributed to the consideration of the constraint from hydrogen bond formation between the citrate molecule and the oxygen atoms in the oxalate group within the crystal steps. In comparison, the binding energy is only −59.8 kJ mol^{-1} for the step with the oxalate groups parallel to the basal plane. This smaller value occurs because now the oxalate groups on both the riser and the basal plane are pointing away from the step. The optimal configuration for the first case is shown in Figure 7a. For the obtuse step, there are also two possible ways for the oxalate group to be expressed at the step edge, either parallel or perpendicular to the (010) plane. However, the former structure is less probable because there are no cations associated with oxalate groups in the riser plane. Such a structure must have a short lifetime and quickly evolves to the latter structure with a binding energy of −92.8 kJ mol^{-1}. From the combined AFM measurements and molecular modeling calculations of the

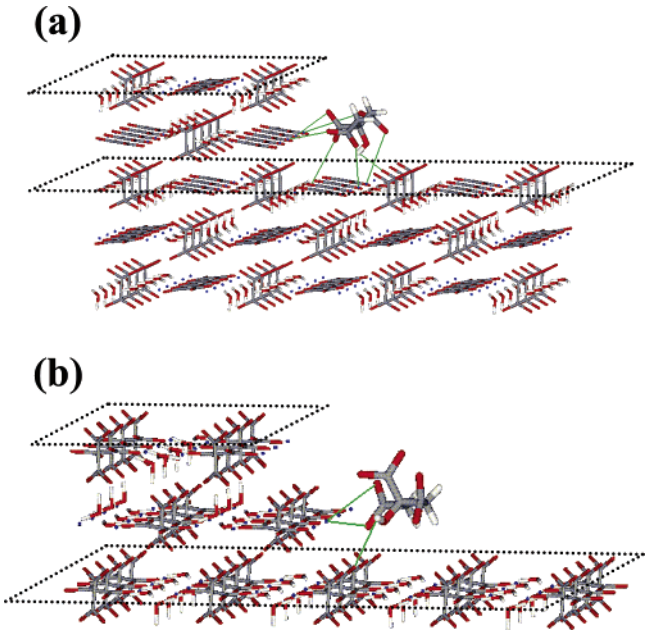

Figure 7. Geometry of citrate bound to the steps on the (010) face in the minimum energy configuration. Note that the oxalate groups extend beyond the (010) plane. Although the steps on the (010) plane are quadruple, for clarity, only the double step configurations are shown. (a) Citrate molecule bound to the [100] step; (b) citrate molecule bound to the [021] step.

binding energy, we conclude that the [100] step is most likely to be the square step.

We also calculated the binding energies of citrate binding to the ⟨021⟩ steps on the (010) plane. As with the [100] step, this step can be either square or obtuse depending on the step riser orientation. The binding energy for the square step is −102.4 kJ mol^{-1}, but it is only −56.9 kJ mol^{-1} if the step is obtuse. Because AFM images showed that citrate had little effect on this step, a smaller binding energy is more reasonable. Thus, the [021] step is most likely to be obtuse. The minimum energy configuration of citrate bounds to the [021] obtuse step is shown in Figure 7b. Because both oxalate groups within the step extend beyond the planes in which they reside, the (021) and (010) planes, they produce strong electrostatic repulsions to carboxylic groups within citrate molecules. Consequently, two of the carboxylic groups turn away from the steps, while the third carboxylic group binds to the calcium ion in the step riser. Similar to the interaction at the [100] step on the ($\bar{1}$01) face, the hydroxyl group forms an H-bond with the oxalate group in the basal plane.

Comparing all of the modeling results, we find that the predicted binding energies of citrate to the steps on these two faces are very consistent with the AFM results. On the ($\bar{1}$01) face, binding energies to the acute [101] and [120]/[1$\bar{2}$0] steps are very high, −166.5 and −162.4 kJ mol^{-1}, respectively, and these are the step directions that become most inhibited and roughened. Binding to the [$\bar{1}\bar{2}$0]/[$\bar{1}$20] steps is intermediate in strength (−133.8 kJ mol^{-1}), and, although these steps are slowed and become roughened, the strength of the inhibition is much less than for the other step directions on this face. On the (010) face, binding to all steps is much less than for all of the steps on the ($\bar{1}$01) face, ranging from −56.9 to −102.4 kJ mol^{-1}, and these steps are only slightly affected by addition of citrate. For both the ($\bar{1}$01) and the (010) faces, binding to flat terraces is the weakest of all, being −65.4 and −48.9 kJ mol^{-1}, respectively. On the basis of these comparisons, we conclude that values of the binding energy in excess of approximately −100 to −120 kJ mol^{-1} are required to significantly influence step kinetics and morphology on COM.

These discussions of molecular modeling have not considered hydration of any ions during crystal growth. However, conclusions drawn from this constant dielectric model can be used to develop insights into the interaction of citrate with crystal surfaces. Because ion hydration mainly attenuates electrostatic interactions among ions in solution, such attenuation will be similar for all ions and the effect on the calculations can roughly be treated as a scaling factor. Thus, the differences in binding energy for the various configurations should still hold.

Conclusion

Our AFM results are consistent with the molecular modeling calculations; that is, citrate modifies the shape and inhibits the growth of COM crystals by selectively pinning step motions on the ($\bar{1}$01) face. The selective binding results in anisotropic step kinetics that directly determines the modification in crystal shape. The selectivity is imposed by stereochemical characteristics of citrate molecules that require multiple binding sites for the three carboxylic acid groups when interacting with crystal surfaces. Furthermore, hydrogen bond formation between the citrate hydroxyl group and the oxygen atom within the crystal plane plays a pivotal role in stabilizing the attachment during growth. In addition, the electrostatic repulsion between the ends of the oxalate molecules and the carboxyl groups plays a large role in limiting the binding of citrate to steps on the (010) face.

Our results show that COM modification by citrate is due to changes in step kinetics rooted in the thermodynamics of citrate−step interactions. The differential citrate−step interaction leads to anisotropic inhibition of step motion on adjacent faces and rounding of steps on the dominant face. These changes are directly translated into the bulk crystal habit. Because the citrate molecule contains multiple carboxylic acids and a hydroxyl group, the results gained from our study provide insights into shape modification of other biogenic crystals by macromolecules such as polypeptides or proteins. On the other hand, because citrate only strongly inhibits the growth of COM crystal on one specific face, leaving the (010) to grow uninhibited, our results suggest that additional therapeutic agents are needed for optimal therapy of kidney stone disease.

Acknowledgment. This work was performed under the auspices of the U.S. Department of Energy by the University of California, Lawrence Livermore National Laboratory, under Contract No. W-7405-Eng-48. We thank the support from the U.S. National Institutes of Health through Grants DK61673 and DK33501.

JA043591S